www.elsevier.com/locate/memsci

Comprehensive study on PVDF-HFP/BMImBF$_4$/AgBF$_4$ membranes for propylene purification

Raúl Zarca, Antoniel Carlos C. Campos, Alfredo Ortiz, Daniel Gorri, Inmaculada Ortiz

PII: S0376-7388(18)32575-4
DOI: https://doi.org/10.1016/j.memsci.2018.11.023
Reference: MEMSCI16625

To appear in: *Journal of Membrane Science*

Received date: 14 September 2018
Revised date: 2 November 2018
Accepted date: 10 November 2018

Cite this article as: Raúl Zarca, Antoniel Carlos C. Campos, Alfredo Ortiz, Daniel Gorri and Inmaculada Ortiz, Comprehensive study on PVDF-HFP/BMImBF$_4$/AgBF$_4$ membranes for propylene purification, *Journal of Membrane Science,* https://doi.org/10.1016/j.memsci.2018.11.023

Comprehensive study on PVDF-HFP/$BMImBF_4$/$AgBF_4$ membranes for propylene purification

Authors: Raúl Zarca[1], Antoniel Carlos C. Campos[2], Alfredo Ortiz[1], Daniel Gorri[1], Inmaculada Ortiz[1*]

[1]Department of Chemical and Biomolecular Engineering. University of Cantabria, Av. Los Castros 46, 39005 Santander, Spain

[2]Institute of Chemistry, Rio de Janeiro State University (UERJ), Campus Maracanã, P H L C, São Francisco Xavier St., 524, Rio de Janeiro, RJ, Brazil, 20550-900.

[*]Corresponding author: ortizi@unican.es

Abstract

In this work, a comprehensive analysis of PVDF-HFP/$BMImBF_4$/$AgBF_4$ facilitated transport membranes for olefin/paraffin separation is presented. Previous works of our research group have reported high flux and propylene selectivity under dry conditions and using synthetic gas mixtures, highlighting the promising potential of these membranes for industrial applications. This work advances in the understanding of the phenomena involved in membrane performance and moves one step forward in the knowledge of the industrial viability of this membrane system. First, the internal interactions between the silver cations and the polymer backbone, the silver salt dissociation and the silver degradation have been studied using FTIR, Raman and XPS spectroscopic techniques. Secondly, the experimental membrane performance during 110 days and working at changing relative humidity conditions in the feed gas has been assessed. Thermogravimetric techniques helped determining the water uptake capability of the facilitated transport membrane. Thirdly, real gas mixtures from a fluid catalytic cracking unit were provided by the industry and used in permeation experiments to check the membrane behavior under industrial-like conditions. The results provide

experimental evidence for the previously theorized facilitated transport mechanisms and reveal a major influence of feed gas humidity on membrane performance. On the other hand, the industrial gas mixture produces no deviation from synthetic feed conditions due to trace contaminants. Finally, the carrier deactivation in long-term permeation has been quantified through a mathematical expression.

Keywords

Propylene, membrane, facilitated transport, humidity, real gas mixture, silver degradation.

1. Introduction

The separation of propane/propylene mixtures is one of the most costly processes in the petrochemical industry, caused by the similar physicochemical properties of both species, which requires the use of energy intensive cryogenic or high pressure distillation [1]. Among the most promising alternatives to traditional distillation, membrane technology offers a compact, modular and simple operation, allowing for process intensification [2]. In the last years, facilitated transport membranes have demonstrated exceptional separation performance in terms of permeability and selectivity [3]. These membranes make use of transition metal cations, typically silver, that can selectively and reversibly react with the olefin according to the Dewar-Chatt-Duncanson model [4,5]. This principle has been implemented in different configurations in recent times. The most basic approach consists in filling the pores of a polymeric support with a liquid solution of the carrier salt. However, this supported liquid membranes (SLM) lack from stability due to solvent evaporation and dragging [6–9]. Although the use of novel ionic liquids has overcome the solvent evaporation problems, the expelling out of solvent from the pores due to the transmembrane

pressure is still a major drawback [10–13]. Proper mechanical stability and separation performance can be achieved combining the properties of dense membranes with facilitated transport through the synthesis of polymer/salt systems. In these systems, the silver salt is dissolved along with the polymer and the membrane is then fabricated through solvent casting [14], which results in a dense facilitated transport membrane usually described as a polymer electrolyte [15–17]. The internal structure and olefin/paraffin separation performance of these systems have been studied rather extensively in oxygen-containing polar polymers such as poly(2-oxazoline) POZ, poly(vinyl alcohol) (PVA) and poly(vinyl pyrrolidone) (PVP) [18–20]. Additionally, several studies have assessed the potential of these electrolytes for energy applications using fluoropolymers and lithium salt blends [21,22]. However, deeper knowledge on fluoropolymer-silver salt interactions is required in order to fully understand its gas separation potential.

In this regard, recent works of our research group have demonstrated the promising performance of fluoropolymer/silver salt membranes containing imidazolium based ionic liquids [23–25]. The presence of the ionic liquid, a non-volatile additive, serves two purposes: it helps stabilizing the silver cations, partially mitigating the carrier deactivation issues [5,26,27], and it acts as a fluid medium that enables mobile carrier transport. In these works, 1-butyl-3-methylimidazolium tetrafluoroborate ($BMImBF_4$) ionic liquid is used for its affinity to olefinic compounds and for having the same anion as the silver salt, which reduces the system complexity [28]. Poly(vinylidene fluoride-co-hexafluoropropylene) PVDF-HFP is selected for its high thermal, chemical and mechanical stability. In addition, it contains fluorine atoms that are likely to form weak interactions with the Ag^+ cations according to the Pearson's Hard-Soft–Acid-Base (HSAB) theory [29], which gives rise to fixed site carrier transport. $AgBF_4$ is used as

carrier precursor because the lattice energy of BF_4^- anion is low enough to allow the olefin-silver complexation [30]. However, the internal interactions caused by the complexity of this membrane system and its responses to changes in the feed humidity conditions are still unclear. Furthermore, few studies assess the performance of silver-containing membranes in the long-term, and what is more important, there is a lack of information regarding permeation of real gas mixtures provided by the industry, which is especially critical given the instability issues caused by silver reduction.

In this work, the internal structure of the PVDF-HFP/$BMImBF_4$/$AgBF_4$ membrane is assessed implementing various spectroscopic techniques. Moreover, the long-term membrane stability is studied performing a 110 days-long permeation experiment, and the influence of the feed relative humidity on the membrane performance is explored and quantified by modifying the feed humidification conditions. Finally, the behavior of these membranes under real conditions is studied permeating a FCC refinery gas mixture provided by the industry.

2. Experimental

2.1 Chemicals

Propylene and propane were supplied by Praxair with a purity of 99.5%. Poly(vinylidene fluoride-co-hexafluoropropylene) (PVDF-HFP) was purchased from Sigma Aldrich. 1-Butyl-3-methylimidazolium tetrafluoroborate ($BMImBF_4$) with a minimum purity of 99% and halide content of less than 500 ppm was supplied by Iolitec. Silver tetrafluoroborate ($AgBF_4$) with a minimum purity of 99% was supplied by Apollo Scientific Ltd. Tetrahydrofuran (THF) purchased from Panreac was used as solvent for membrane synthesis. The industrial propane/propylene gas mixture was

kindly provided by Petronor S.A. All chemicals were used as received without further purification.

2.2 Membrane synthesis

The facilitated transport membranes studied in this work have been synthesized using the solvent casting method described in previous works [24,25]. The resulting membrane thickness is roughly 100 μm. The real thickness of each specific membrane has been measured with a Mitutoyo Digimatic MDC-25SX (accuracy ± 0.001 mm) digital micrometer and used for calculation purposes. The membrane composition of the studied membranes consist of 0.8g of PVDF-HFP, 0.2g of $BMImBF_4$ and 0.6g of $AgBF_4$. In the polymer/salt membranes the ionic liquid addition has been omitted.

2.3 Gas permeation experiments

A continuous-flow permeation technique has been used for the permeation experiments. A detailed description of this technique and the experimental apparatus can be found in previous works [23]. Briefly, mass flow controllers are used to generate a feed mixture that is further introduced in the upper chamber of a permeation cell where the membrane is located. Nitrogen is used as sweeping gas in the lower chamber and the permeate and retentate streams are then analyzed using gas chromatography to determine the transmembrane flux of each species. However, for humidified feed testing the experimental apparatus has been modified with the set-up depicted in Figure 1, which allows generating any desired relative humidity in the feed stream by controlling the ratio of dry to humidified feed.

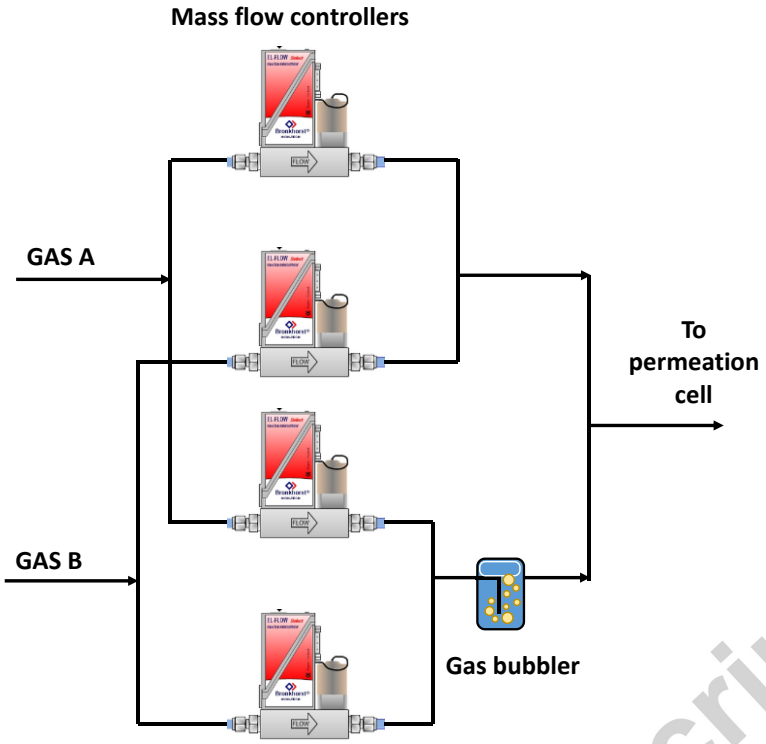

Figure 1. Set-up for relative humidity control.

The permeation experiments where conducted at the experimental conditions shown in Table 1.

Table 1. Experimental conditions

Experimental condition	Value
T (K)	298
Permeation area (cm^2)	53
N_2 flow ($mL\ min^{-1}$)	20-40
C_3H_6 flow ($mL\ min^{-1}$)	20
C_3H_8 flow ($mL\ min^{-1}$)	20
C_3H_8 /C_3H_6 feed gas ratio	50:50
Feed side pressure (bar)	1.2
Permeate side pressure (bar)	1

2.4 Membrane characterization techniques

Different characterization techniques were implemented to assess the internal structure, water uptake capability and carrier degradation of the facilitated transport membranes. TGA analysis were performed using a TG-DTA 60H Shimadzu thermobalance and Fourier transform infrared (FTIR) spectra were recorded using a Perkin Elmer Spectrum Two spectrometer. Additionally, Raman spectroscopy was carried out using a Horiba T64000 triple spectrometer equipped with a confocal microscope and a Jobin Yvon Symphony CCD detector cooled with liquid nitrogen. A 488 nm beam from a Kr-Ar ion laser was focused through a 100x objective, using 2 mW laser power in all measurements. The spectral curves were fitted using Lorentzian functions. Finally, XPS spectra were acquired using an SPECS (Berlin, Germany) X-ray photoelectron spectrometer. The samples were analyzed using an Mg anode operated at 225 W (E=1253.6 eV, 13 kV, 17.5 mA). The carbon (C 1s) line at 284.8 eV was used as the reference in our determinations of the binding energies of the silver. A scanning interval of 0.1 eV was used for the final spectrum acquisition.

3. Results

3.1 Thermogravimetric analysis

The thermal analysis has been performed to assess the potential water uptake of the studied membranes. Figure 2 displays the thermogravimetric curves of PVDF-HFP, PVDF-HFP/$AgBF_4$ and PVDF-HFP/$BMImBF_4$/$AgBF_4$ membranes.

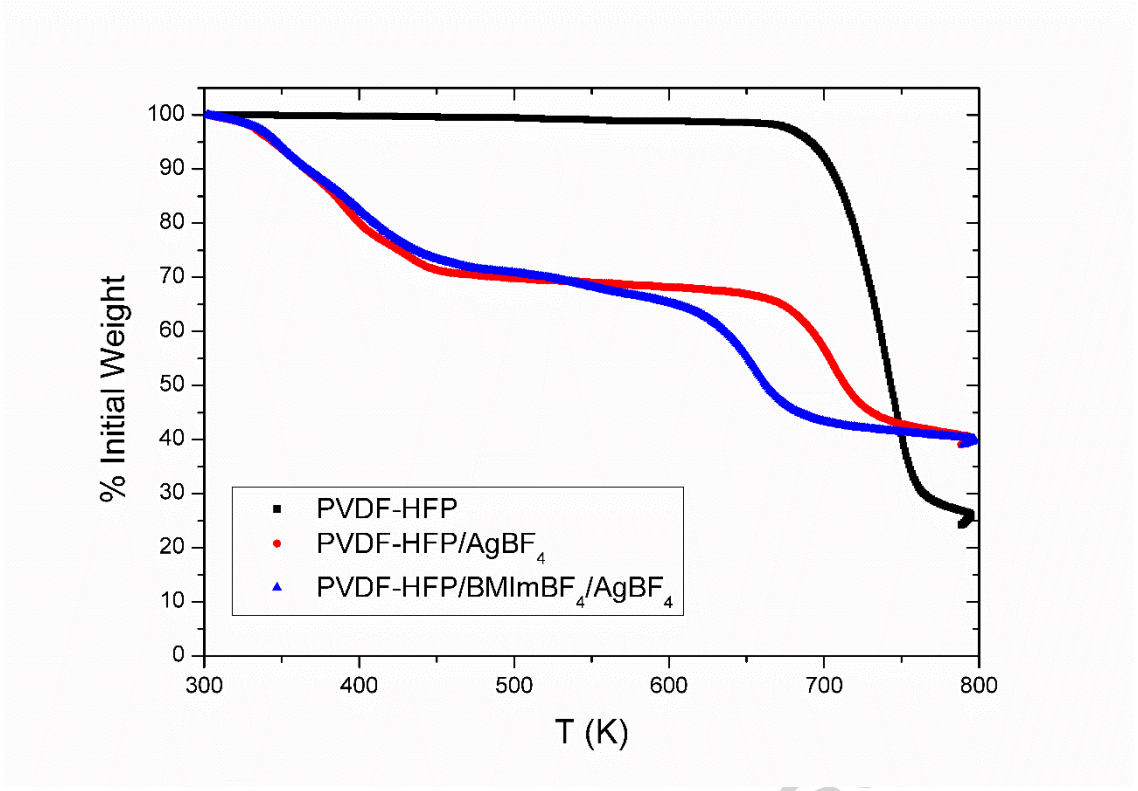

Figure 2. TGA curves of the studied membranes.

The membrane samples were vacuum dried at 30 mbar and 298 K for 24 hours after casting to completely remove the remaining solvent. Prior to testing the samples were exposed to ambient moisture (~80% RH at room temperature) for 24 hours. In this manner, any water loss appearing at the beginning of the temperature ramp can be attributed to water evaporation. According to Figure 2, the pure polymer membrane exhibits no weight loss until it reaches its degradation temperature around 680 K, which reveals no water uptake. This is in good agreement with the hydrophobic nature of the fluoropolymer [31]. However, Figure 2 shows prominent mass losses of the silver-containing membranes in the 300-436 K temperature range. Thus, it can be concluded that the addition of the $AgBF_4$ salt to the membrane composition dramatically changes the nature of the facilitated transport membranes due to its high hygroscopicity, which results in water uptakes of around 25 wt% when exposed to moist conditions. The PVDF-HFP/$BMImBF_4$/$AgBF_4$ membrane starts degrading at 625 K, slightly below the

pristine PVDF-HFP and PVDF-HFP/$AgBF_4$ membranes. This is caused by the influence of the ionic liquid on the polymer structure, which yields a multistep decomposition mechanism, as reported by Shalu et al. [32].

3.2 Fourier transform infrared spectroscopy (FTIR)

The interaction between the Ag^+ cations and the fluorine atoms of the polymer chains can be studied through infrared spectroscopy analyzing the polymer CF_2 symmetrical stretching mode and comparing that of the pure polymer with the silver-containing membranes, see Figure 3.

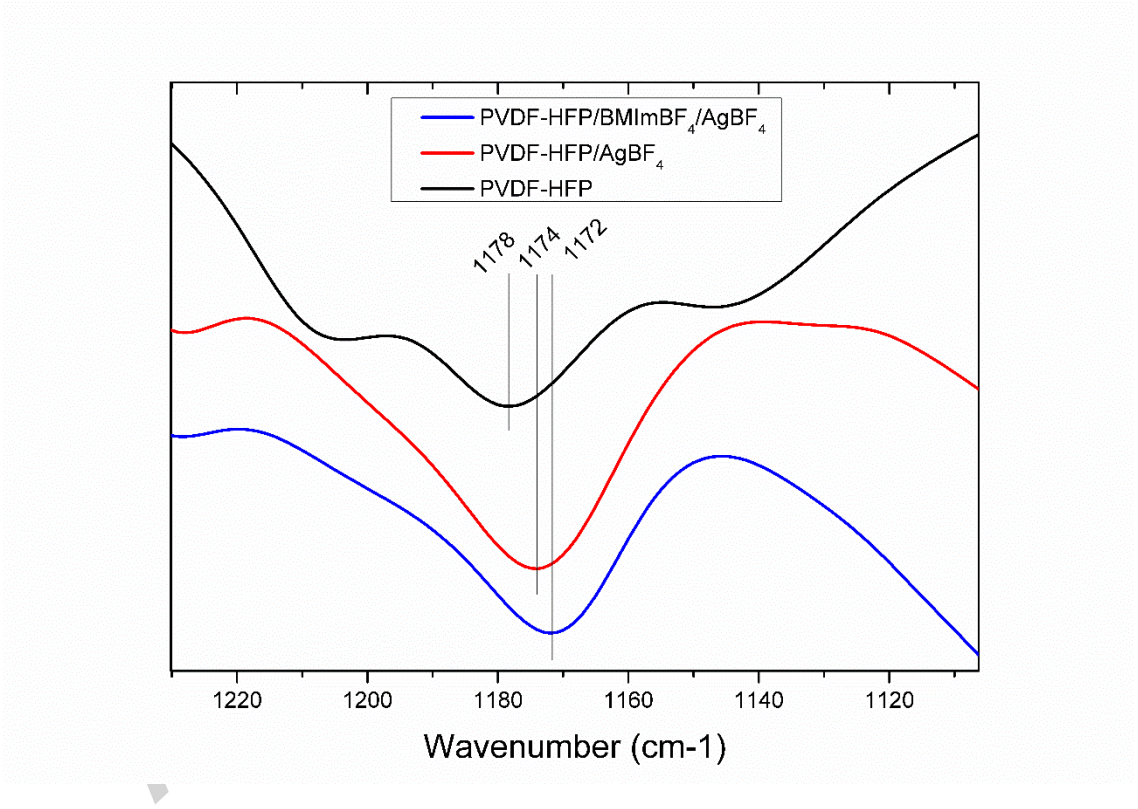

Figure 3. FTIR spectra of the studied membranes.

The CF_2 peak of the pure polymer appears in the 1178 cm^{-1} band. After incorporation of the silver salt, the stretching band shifted to 1174 and 1172 cm^{-1} in the PVDF-HFP/$AgBF_4$ and PVDF-HFP/$BMImBF_4$/$AgBF_4$ respectively. Previous works on PVDF-HFP/HBF_4 and POZ/$AgBF_4$ polymer electrolytes found that this shift to lower

wavenumber indicates a weakening of the polymer heteroatom bonding (i.e. C-F and C=O, respectively), which is caused by the interaction between these heteroatoms and the cations (i.e. H^+ and Ag^+, respectively) [18,33]. According to these findings it can be concluded that the wavenumber shift observed in this work for the CF_2 groups is also related to the weakening of the C-F bond caused by the interaction of silver cations with the fluorine atoms of the PVDF-HFP, which is the basis of the fixed site carrier transport mechanism.

3.3 RAMAN spectroscopy

Better insight on the $AgBF_4$ dissociation behavior can be achieved using Raman spectroscopy to analyze the regions of the BF_4^- stretching bands in the pure $AgBF_4$, and the silver-containing membranes. Figure 4 shows the BF_4^- stretching band region of PVDF-HFP/$AgBF_4$ and PVDF-HFP/$BMImBF_4$/$AgBF_4$ membranes. The symmetric stretching mode of BF_4^- has been previously reported at 774 cm^{-1} in the pure $AgBF_4$ [34] and in the pure $BMImBF_4$ [35]. However, the spectra in Figure 4 shows a wavenumber shift to ~767 cm^{-1} in both membranes. According to previous studies, this wavenumber corresponds to BF_4^- free ions [20,35], which means that this change in the Raman spectra is due to an effective $AgBF_4$ dissociation [36].

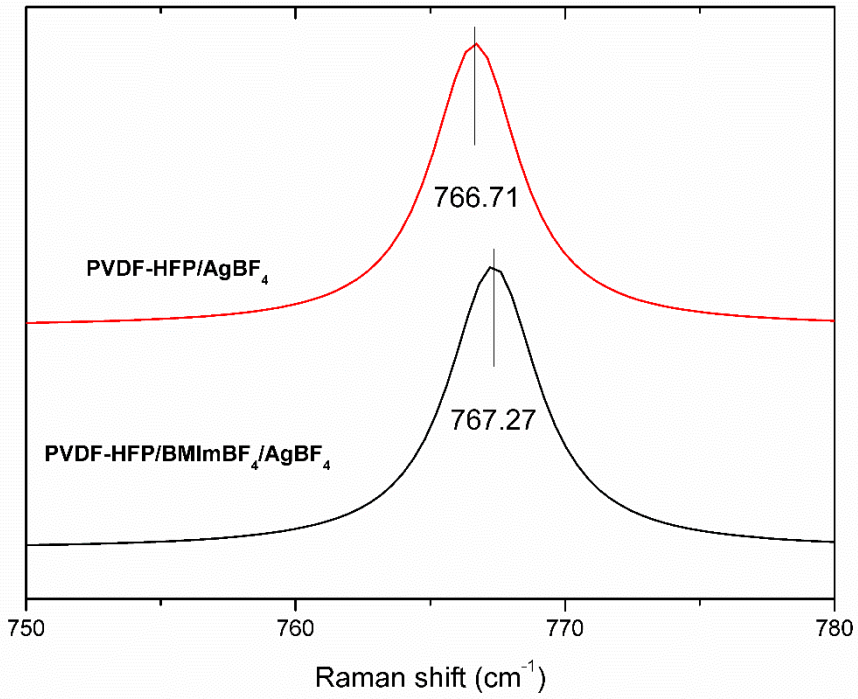

Figure 4. Raman spectra of PVDF-HFP /$AgBF_4$ and PVDF-HFP/$BMImBF_4$/$AgBF_4$ membranes.

These evidences provided by the Raman spectroscopy support the FTIR results on polymer-silver interactions and suggest that the silver salt dissolution in the ionic liquid-containing membrane is caused not only by the polymer backbone but also by the non-complexed ionic liquid [23], which explains the existence of silver cations with certain mobility to act as mobile carriers.

3.4 X-ray photoelectron spectroscopy (XPS)

X-ray photoelectron spectroscopy has been used to expand the knowledge on membrane structure and degradation. The Ag 3d regions of the XPS spectra can confirm the interactions between the silver cations and the polymer fluorine atoms. Figure 5 shows the XPS spectra of a PVDF-HFP/$BMImBF_4$/$AgBF_4$ composite membrane after a long term permeation experiment (110 days). Table 2 summarizes the two silver species

observable after signal deconvolution. The Ag 3d5/2 band of pure $AgBF_4$ has been previously reported at 369.2 eV. However, in the composite membrane, the binding energy has shifted to 368.47 eV. This reduction in the photoelectron binding energy is caused by the coordination between the silver atoms and the polymer backbone as demonstrated by Kim et al (2012), who found the same phenomenon for several $AgBF_4$/polymer blends [37]. Additionally, a second silver species (Ag 3d5/2=368.26 Ag 3d3/2=374.25) is associated with the presence of metallic silver [38], presumably due to the silver reduction caused by the long term permeation test.

Table 2. XPS regions of PVDF-HFP/BMImBF$_4$/AgBF$_4$ membrane after permeation test.

	Region	Position
Species A	Ag 3d 5/2	368.47
	Ag 3d 3/2	374.54
Species B	Ag 3d 5/2	368.26
	Ag 3d 3/2	374.25

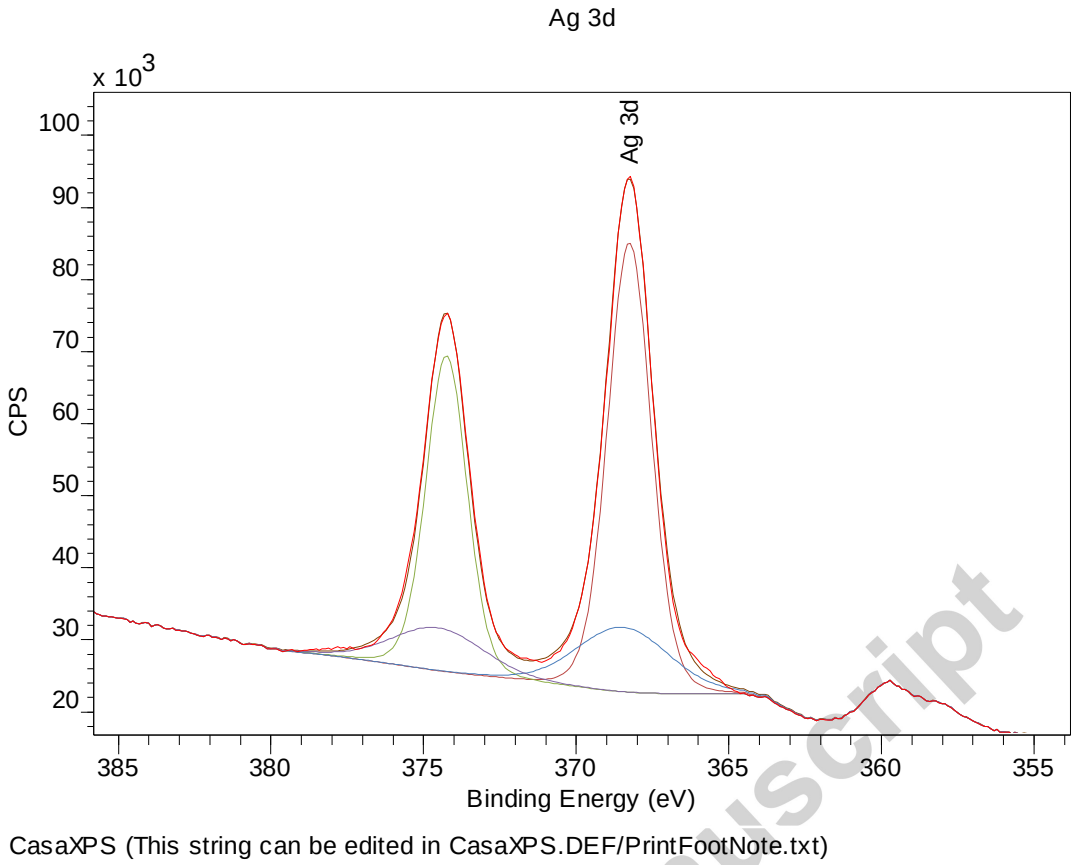

Figure 5. XPS spectra of the PVDF-HFP/BMImBF$_4$/AgBF$_4$ membrane after permeation test.

3.5 Long-term permeation under humid conditions

Figure 6 shows a 110 days long-term permeation test on a PVDF-HFP/BMImBF$_4$/AgBF$_4$ facilitated transport composite membrane. The feed gas consisted of an equimolar propane/propylene mixture at 1.2 bar total pressure. The main goal of this experiment is to determine the separation behavior of a composite membrane over an extended period of time, assessing both the feed gas relative humidity effect and the possible loss of performance due to carrier deactivation. Figure 6 is divided into five sections (**I-V**) accounting for the relative humidity conditions and following the sequence of the experimental runs. A characteristic feature of this facilitated transport membranes under dry conditions is a sharp decrease of the

permeation flux in the first operating hours ostensibly caused by the rapid loss of water and residual solvent by evaporation, Figure 7 (section **II**). At the beginning of the test (section **I**) the humidity was kept at saturation and no flux decay was observed during the first 5 days, which confirms that the characteristic curve observed under dry gas conditions is due to solvent and water moisture evaporation. From day 5 to day 27 some instability in membrane performance occurred due to controlled changes in the temperature and pressure conditions within the experiments. In Figure 6 this is more

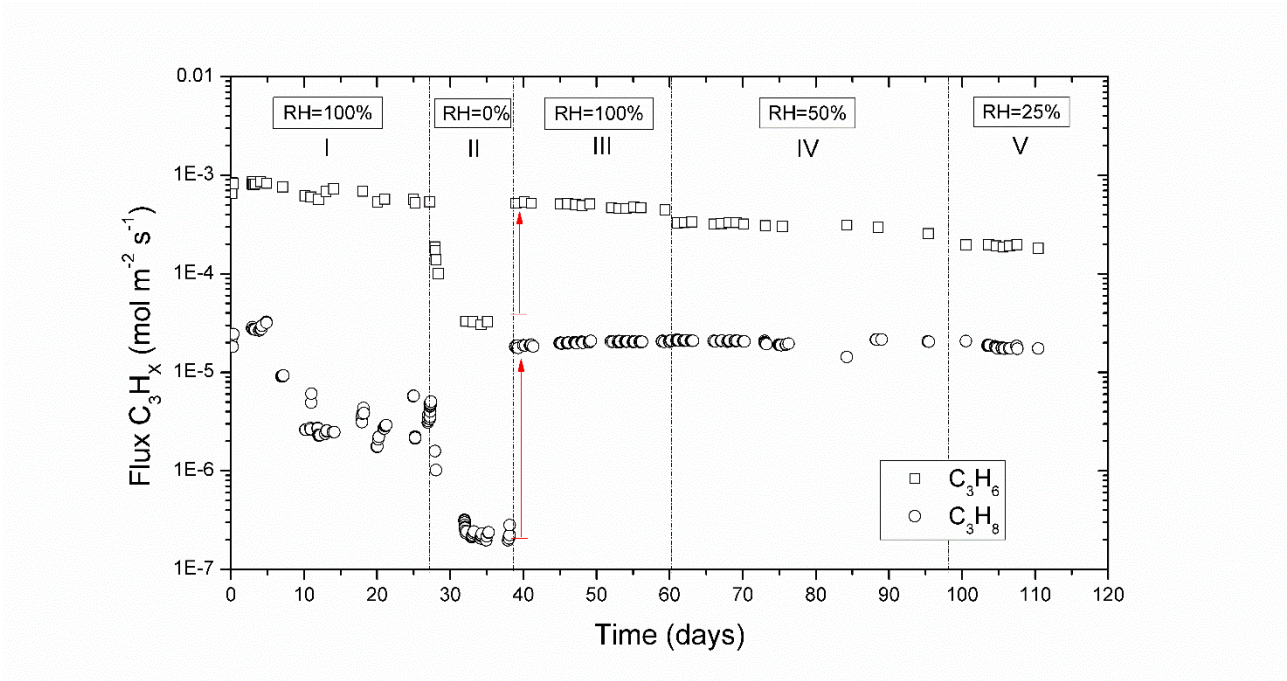

evident for the propane flux due to the semi-logarithmic scale.

Figure 6. Long term permeation experiment of PVDF-HFP/BMImBF$_4$/AgBF$_4$ composite membrane at 298 K and 1.2 bar feed pressure (C_3H_8/C_3H_6 50:50) under different relative humidity conditions.

After 27 days, during section **II**, the feed was changed to dry gases, which resulted in a major propane and propylene transmembrane flux decrease as water evaporation

occurred within the membrane. A detailed depiction of the drying curve is shown in Figure 7.

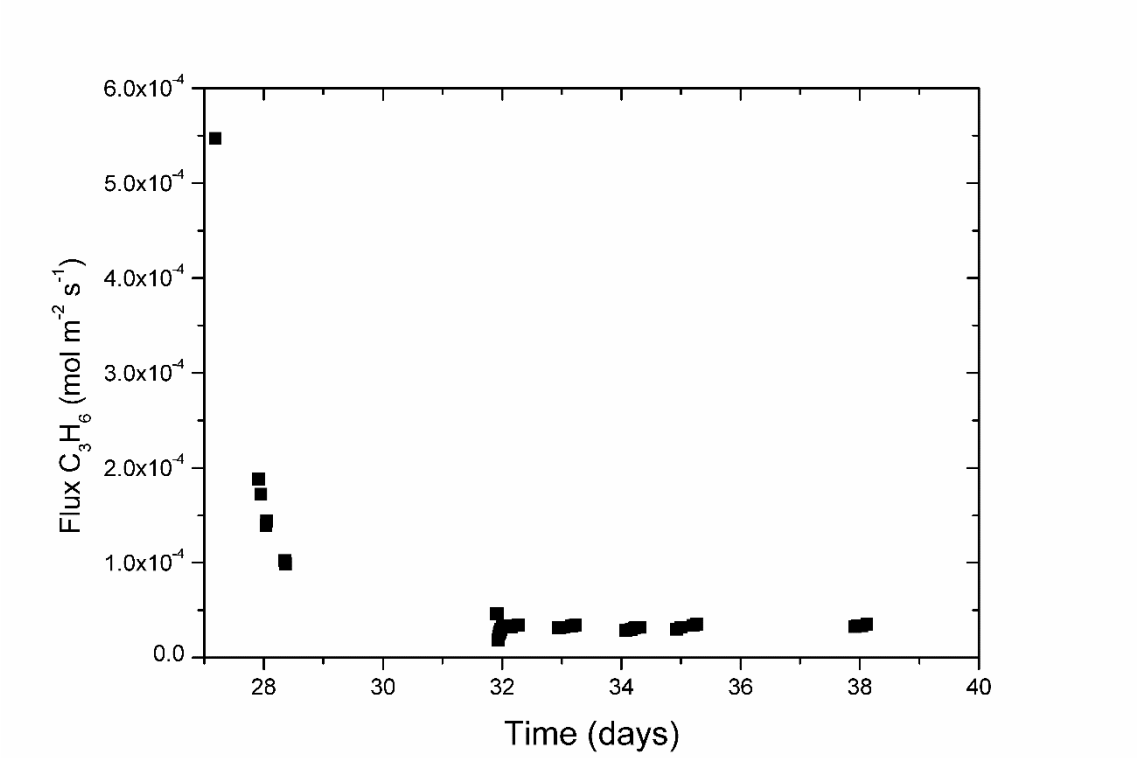

*Figure 7. Propylene transmembrane flux decrease in section **II**.*

When the humidified gas mixture was fed again into the system (section **III**), the flux increase of both gaseous species was almost immediate, reaching the flux values attained prior to drying. This abrupt increase, noted with red arrows in Figure 6, reveals the exceptional capability of these membranes to absorb water from the environment. During sections **III**, **IV** and **V** a feed gas relative humidity of 100, 50 and 25% was used, respectively. These variations in the humidity conditions resulted in moderate changes in the propylene transmembrane flux while the propane flux remained almost constant at its highest level.

However, it should be noted that, apart from the humidity influence, the propylene transmembrane flux undergoes a continuous slight decrease, evidenced by a constant

slope in Figure 6. On the contrary, the propane flux does not suffer such decrease, which suggests that this phenomenon is caused by carrier deactivation. Furthermore, it was possible to quantify the deactivation rate by fitting the data for each section (**I-V**), to an exponential curve, which yielded the following expression:

$$J_{C_3H_6}(t) = J_{C_3H_6}(t_0) \cdot e^{-5.5x10^{-3} \cdot t} \quad (1)$$

where $J_{C_3H_6}(t_0)$ is the initial propylene transmembrane flux at a given temperature, pressure and relative humidity conditions and the time *t* is introduced in days. This expression allows for membrane lifetime calculation if a minimum required performance is established.

This carrier deactivation prevents from fitting a mathematical expression for the propylene flux dependency on relative humidity because each experimental section has been obtained at different times and, consequently, the propylene flux is not only affected by the relative humidity but also by the elapsed time from the start of the experiment. However, using Equation 1, it was possible to project the propylene flux values to a common initial point. Finally, combining a mathematical expression for the drying curve (Figure 7) with the propylene flux at each relative humidity, it was possible to obtain a fitting curve for the propylene transmembrane flux as a function of the relative humidity (Eq. 2), Figure 8.

$$J_{C_3H_6}(RH) = 5.82x10^{-5} RH^{0.49} \quad (2)$$

Figure 8 evidences a sharp increase in the propylene flux with the relative humidity for RH<10% and a smooth increase after that value (dash line in Figure 8); this finding supports the fact that even with a low relative humidity in the gaseous feed stream it is possible to produce severe enhancements of the propylene transmembrane flux. A

similar trend has been reported by Catalano et al. (2012) for oxygen and nitrogen permeation in PFSI membranes [39].

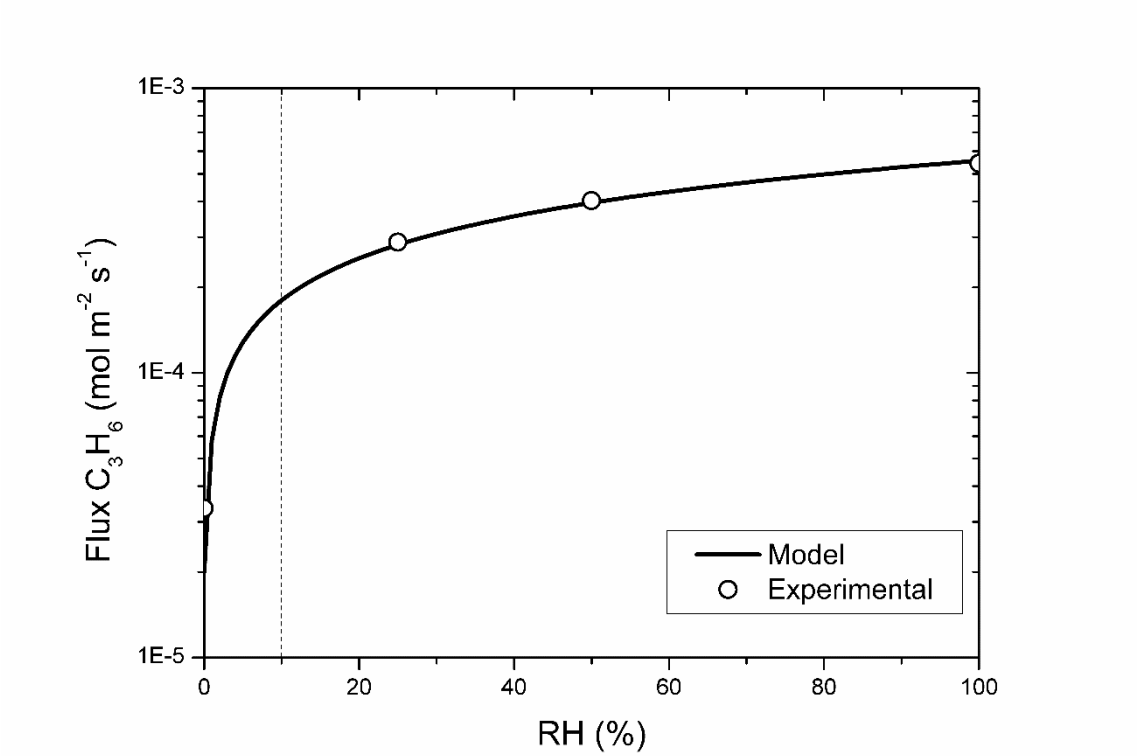

Figure 8. Experimental data and mathematical regression for the dependency of the propylene transmembrane flux on the relative humidity.

Finally, Table 3 displays the permeability and selectivity values of the facilitated transport membrane for each relative humidity condition. The humidification of the feed gases produces major changes in the membrane performance, reducing the selectivity and increasing the permeability of both the olefin and the paraffin. This is a characteristic effect of water vapor-induced swelling [40,41]. The enlargement of the polymer free volume caused by the water uptake increases the diffusivity of the gaseous species and the propylene-silver complex, which leads to notable permeability values but at the expense of membrane selectivity.

Table 3. Average permeability and selectivity values of the PVDF-HFP/BMImBF$_4$/AgBF$_4$ membrane for each relative humidity during the long-term permeation test.

RH (%)	P C_3H_8 (Barrer)[a]	P C_3H_6 (Barrer) [a]	α C_3H_6/C_3H_8 (-)
0	1.2	172	144
25	97.3	1032	11
50	107.6	1666	16
100	106.5	2555	24

[a] 1 Barrer = 10^{-10} cm^3 (STP) cm cm^{-2} s^{-1} $cmHg^{-1}$.

Although membrane swelling is usually responsible for lowering the polymeric membranes selectivity below the industrially required values, in this case, the selectivity remains high enough to consider humid operation as a useful tool to tailor the permeability-selectivity trade-off. Thus, wet gas could be implemented as a controlling agent when productivity is preferred over product purity. In this way, multistage membrane processes performing a refining separation after a bulk concentration could modulate the purity-productivity trade-off in each stage by controlling the feed gas relative humidity [42].

3.6 Industrial gas mixture permeation test

Figure 9 shows the facilitated transport membrane performance when the feed consists of a real propane/propylene mixture compared with a synthetic gas mixture. The industrial gas mixture is the product stream of a fluid catalytic cracking unit and its composition is displayed in Table 4. It mostly consists of a propane/propylene mixture (25:75) containing minor quantities of light paraffins and olefins.

Table 4. Industrial gas mixture composition.

Component	Concentration (mol%)
Methane	0.0034
Ethane	0.1503
Ethylene	0.0099
Propane	24.8837
Propylene	74.7208
Isobutane	0.1872
N-butane	0.0016
Trans-butene	0.0214
Iso-butene	0.0218
Hydrogen sulfide	< 0.2 ppm
Acetylene	< 0.2 ppm
Hydrogen	< 0.2 ppm

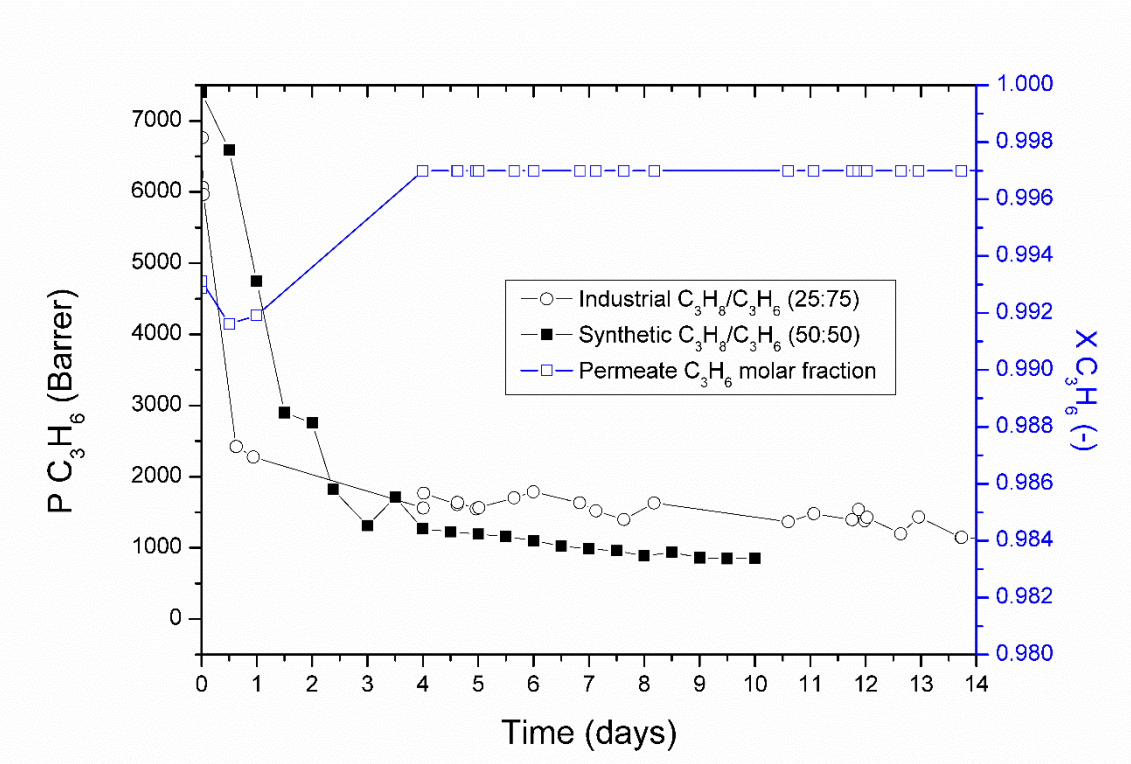

Figure 9. Synthetic and industrial gas mixture permeation experiments on a PVDF-HFP/BMImBF$_4$/AgBF$_4$ membrane under dry conditions at 298 K and 1.2 bar total feed pressure.

Given that both feeds differ in composition, permeability, which is normalized by the partial pressure gradient, has been plotted instead of the transmembrane flux. Both permeation experiments have been performed under dry conditions to simulate refinery conditions, hence, both suffer the characteristic permeability decrease due to solvent and water evaporation in the first hours of operation. Since the propylene transmembrane flux is similar in both cases, Figure 9 evidences that the membrane performance is not affected by known contaminant trace components potentially present in industrial streams (i.e. acetylene, hydrogen sulfide and hydrogen [43]) during the experiment extent.

Focusing on the industrial gas mixture, after 4 days (along the flat section of Figure 9) the relative propylene concentration achieved in the permeate side (i.e. subtracting the sweep gas concentration) is roughly 99.7 mol.%, which equals the purity obtained with synthetic gas mixtures. These results confirm that the prominent separation performance of the studied membranes is not restricted to laboratory conditions with synthetic gas mixtures and demonstrate the suitability of these composite facilitated transport membranes to treat real feed streams.

4. Conclusions

The spectroscopic characterization of PVDF-HFP/$BMImBF_4$/$AgBF_4$ membranes used in the separation of propane/propylene mixtures confirm the existence of weak interactions between the Ag^+ cations and the fluorine atoms of the polymeric backbone, which along with the addition of ionic liquids result in a hybrid fixed site/mobile carrier transport mechanism yielding high olefin permeability and selectivity. The long-term permeation experiment carried out under changing feed gas humidity conditions revealed a slight permeability decrease due to silver degradation, which is mainly associated to silver reduction, supported by XPS spectra of the used membrane; this loss of membrane activity was observed to be independent of the experimental conditions. Although this degradation is slow enough to allow moderate membrane lifetimes, remediation methods can be further studied to achieve even larger operating periods. On the other hand, the humidification of the feed gas can severely alter the membrane performance, increasing the permeability of the permeant species and decreasing the membrane selectivity due to water vapor-induced swelling. In this regard, thermogravimetric analysis revealed up to 25 wt% membrane water uptake. Since the membrane showed moderate selectivity even at saturation, wet gas could be implemented as a controlling agent when productivity is preferred over product purity. Finally, permeation under real gas conditions revealed no additional degradation caused by minor contaminants that could potentially affect silver stability.

Acknowledgements

Financial support from the Spanish Ministry of Science under the projects CTQ 2015-66078-R and CTQ2016 -75158-R (MINECO, Spain- FEDER 2014–2020) is gratefully acknowledged. Raúl Zarca also thanks the Universidad de Cantabria for the postgraduate fellowship.

References

[1] D.S. Sholl, R.P. Lively, Seven chemical separations to change the world, Nature 532 (2016) 435–437.

[2] J.C. Charpentier, In the frame of globalization and sustainability, process intensification, a path to the future of chemical and process engineering (molecules into money), Chem. Eng. J. 134 (2007) 84–92.

[3] R. Faiz, K. Li, Olefin/paraffin separation using membrane based facilitated transport/chemical absorption techniques, Chem. Eng. Sci. 73 (2012) 261–284.

[4] D.J. Safarik, R.B. Eldridge, Olefin/Paraffin Separations by Reactive Absorption: A Review, Ind. Eng. Chem. Res. 37 (1998) 2571–2581.

[5] A. Ortiz, L.M. Galán, D. Gorri, A.B. De Haan, I. Ortiz, Kinetics of reactive absorption of propylene in RTIL-Ag+ media, Sep. Purif. Technol. 73 (2010) 106–113.

[6] M.T. Ravanchi, T. Kaghazchi, A. Kargari, Supported liquid membrane separation of propylene-propane mixtures using a metal ion carrier, Desalination 250 (2010) 130–135.

[7] S. Azizi, T. Kaghazchi, A. Kargari, Propylene/propane separation using N-methyl pyrrolidone/AgNO3 supported liquid membrane, J. Taiwan Inst. Chem. Eng. 57 (2015) 1–8.

[8] M. Teramoto, H. Matsuyama, T. Yamashiro, Y. Katayama, Separation of Ethylene From Ethane By Supported Liquid Membranes Containing Silver-Nitrate As a Carrier, J. Chem. Eng. Japan. 19 (1986) 419–424.

[9] S. Duan, A. Ito, A. Ohkawa, Separation of propylene/propane mixture by a

supported liquid membrane containing triethylene glycol and a silver salt, J. Memb. Sci. 215 (2003) 53–60.

[10] M. Fallanza, A. Ortiz, D. Gorri, I. Ortiz, Experimental study of the separation of propane/propylene mixtures by supported ionic liquid membranes containing Ag+–RTILs as carrier, Sep. Purif. Technol. 97 (2012) 83–89.

[11] G. Zarca, I. Ortiz, A. Urtiaga, Copper(I)-containing supported ionic liquid membranes for carbon monoxide/nitrogen separation, J. Memb. Sci. 438 (2013) 38–45.

[12] R. Fortunato, C.A.M. Afonso, M.A.M. Reis, J.G. Crespo, Supported liquid membranes using ionic liquids: Study of stability and transport mechanisms, J. Memb. Sci. 242 (2004) 197–209.

[13] P. Scovazzo, Testing and evaluation of room temperature ionic liquid (RTIL) membranes for gas dehumidification, J. Memb. Sci. 355 (2010) 7–17.

[14] R. Zarca, A. Ortiz, D. Gorri, I. Ortiz, Facilitated Transport of Propylene Through Composite Polymer-Ionic Liquid Membranes. Mass Transfer Analysis, Chem. Prod. Process Model. 11 (2016) 77–81.

[15] Y. Yoon, J. Won, Y.S. Kang, Polymer electrolyte membranes containing silver ion for facilitated olefin transport, Macromolecules 33 (2000) 3185–3186.

[16] H. Kataoka, Y. Saito, M. Tabuchi, Y. Wada, T. Sakai, Ionic conduction mechanism of PEO-type polymer electrolytes investigated by the carrier diffusion phenomenon using PGSE-NMR, Macromolecules 35 (2002) 6239–6244.

[17] L. Liu, X. Feng, A. Chakma, Unusual behavior of poly(ethylene oxide)/AgBF4

polymer electrolyte membranes for olefin-paraffin separation, Sep. Purif. Technol. 38 (2004) 255–263.

[18] S.U. Hong, J.H. Jin, J. Won, Y.S. Kang, Polymer-salt complexes containing silver ions and their application to facilitated olefin transport membranes, Adv. Mater. 12 (2000) 968–971.

[19] J.H. Kim, B.R. Min, K.B. Lee, J. Won, Y.S. Kang, Coordination structure of various ligands in crosslinked PVA to silver ions for facilitated olefin transport, Chem. Commun. 2 (2002) 2732–2733.

[20] Y.S. Park, S. Chun, Y.S. Kang, S.W. Kang, Durable poly(vinyl alcohol)/AgBF4/Al(NO3)3 complex membrane with high permeance for propylene/propane separation, Sep. Purif. Technol. 174 (2017) 39–43.

[21] T. Liu, Z. Chang, Y. Yin, K. Chen, Y. Zhang, X. Zhang, The PVDF-HFP gel polymer electrolyte for Li-O2 battery, Solid State Ionics. 318 (2018) 88–94.

[22] S. Abbrent, J. Plestil, D. Hlavata, J. Lindgren, J. Tegenfeldt, Å. Wendsjö, Crystallinity and morphology of PVdF–HFP-based gel electrolytes, Polymer (Guildf). 42 (2001) 1407–1416.

[23] M. Fallanza, A. Ortiz, D. Gorri, I. Ortiz, Polymer-ionic liquid composite membranes for propane/propylene separation by facilitated transport, J. Memb. Sci. 444 (2013) 164–172.

[24] R. Zarca, A. Ortiz, D. Gorri, I. Ortiz, Generalized predictive modeling for facilitated transport membranes accounting for fixed and mobile carriers, J. Memb. Sci. 542 (2017) 168–176.

[25] R. Zarca, A. Ortiz, D. Gorri, I. Ortiz, A practical approach to fixed-site-carrier

facilitated transport modeling for the separation of propylene/propane mixtures through silver-containing polymeric membranes, Sep. Purif. Technol. 180 (2017) 82–89.

[26] A. Ortiz, L. Galán, D. Gorri, A. B. De Haan, I. Ortiz, Reactive Ionic Liquid Media for the Separation of Propylene / Propane Gaseous Mixtures, Ind. Eng. Chem. Res. 49 (2010) 7227–7233.

[27] A. Ortiz, A. Ruiz, D. Gorri, I. Ortiz, Room temperature ionic liquid with silver salt as efficient reaction media for propylene/propane separation: Absorption equilibrium, Sep. Purif. Technol. 63 (2008) 311–318.

[28] M. Fallanza, M. González-Miquel, E. Ruiz, A. Ortiz, D. Gorri, J. Palomar, I. Ortiz, Screening of RTILs for propane/propylene separation using COSMO-RS methodology, Chem. Eng. J. 220 (2013) 284–293.

[29] R.G. Pearson, Hard and Soft Acids and Bases, J. Am. Chem. Soc. 85 (1963) 3533–3539.

[30] C.K. Kim, J. Won, H.S. Kim, Y.S. Kang, H.G. Li, C.K. Kim, Density functional theory studies on the dissociation energies of metallic salts: Relationship between lattice and dissociation energies, J. Comput. Chem. 22 (2001) 827–834.

[31] X. Tian, X. Jiang, Poly(vinylidene fluoride-co-hexafluoropropene) (PVDF-HFP) membranes for ethyl acetate removal from water, J. Hazard. Mater. 153 (2008) 128–135.

[32] Shalu, S.K. Chaurasia, R.K. Singh, S. Chandra, Thermal stability, complexing behavior, and ionic transport of polymeric gel membranes based on polymer PVdF-HFP and ionic liquid, [BMIM][BF4], J. Phys. Chem. B. 117 (2013) 897–

906.

[33] J. Chang, S.W. Kang, CO2 separation through poly(vinylidene fluoride-co-hexafluoropropylene) membrane by selective ion channel formed by tetrafluoroboric acid, Chem. Eng. J. 306 (2016) 1189–1192.

[34] E. Goreshnik, Z. Mazej, X-ray single crystal structure and vibrational spectra of AgBF4, Solid State Sci. 7 (2005) 1225–1229.

[35] D. Ji, Y.S. Kang, S.W. Kang, Accelerated CO2 transport on surface of AgO nanoparticles in ionic liquid BMIMBF4, Sci. Rep. 5 (2015) 16362.

[36] S.W. Kang, K. Char, J.H. Kim, C.K. Kim, Y.S. Kang, Control of ionic interactions in silver salt-polymer complexes with ionic liquids: Implications for facilitated olefin transport, Chem. Mater. 18 (2006) 1789–1794.

[37] J.H. Kim, S.W. Kang, Y.S. Kang, Threshold silver concentration for facilitated olefin transport in polymer/silver salt membranes, J. Polym. Res. 19 (2012) 9753.

[38] T.C. Kaspar, T. Droubay, S.A. Chambers, P.S. Bagus, Spectroscopic Evidence for Ag(III) in Highly Oxidized Silver Films by X-ray Photoelectron Spectroscopy, J. Phys. Chem. C. 114 (2010) 21562–21571.

[39] J. Catalano, T. Myezwa, M.G. De Angelis, M.Giacinti Baschetti, G.C. Sarti, The effect of relative humidity on the gas permeability and swelling in PFSI membranes, Int. J. Hydrogen Energy. 37 (2012) 6308–6316.

[40] W.S. Ho, D.C. Dalrymple, Facilitated transport of olefins in Ag+-containing polymer membranes, J. Memb. Sci. 91 (1994) 13–25.

[41] S. Hong, Effect of water on the facilitated transport of olefins through solid polymer electrolyte membranes, J. Memb. Sci. 181 (2001) 289–293.

[42] R. Zarca, A. Ortiz, D. Gorri, L.T. Biegler, I. Ortiz, Optimized Distillation Coupled With State-of-the-Art Membranes for Propylene Purification, J. Memb. Sci. 556 (2018) 321–328.

[43] T.C. Merkel, R. Blanc, I. Ciobanu, B. Firat, A. Suwarlim, J. Zeid, Silver salt facilitated transport membranes for olefin/paraffin separations: Carrier instability and a novel regeneration method, J. Memb. Sci. 447 (2013) 177–189.

Highlights:

Long term PVDF-HFP/BMImBF$_4$/AgBF$_4$ membrane performance for propylene/propane separation.

The effect of feed humidity, carrier degradation and real gas mixtures has been assessed.

The results confirm the remarkable potential of these membrane to replace distillation.